

# Nonlinear rheology of a dilute emulsion of surfactant-covered spherical drops in time-dependent flows

By P. VLAHOVSKA, J. BŁAWZDZIEWICZ<sup>†</sup>  
AND M. LOEWENBERG

Department of Chemical Engineering, Yale University, New Haven, CT 06520-8286, USA

(Received 4 April 2001 and in revised form 15 January 2002)

The effect of an insoluble surfactant on the rheological behaviour of a dilute emulsion is theoretically studied under low-capillary-number conditions. The dynamics depends on three dimensionless time-scale parameters that characterize the strength of the mechanisms that control the magnitude of the distortion of the surfactant distribution on the drop interface. These mechanisms include Marangoni relaxation, drop rotation by the imposed flow, and oscillations of the imposed flow. The interaction of the time scales gives rise to a complex rheological behaviour. The evolution of the system is described by a nonlinear matrix equation derived by expanding the fluid velocity and surfactant distribution in spherical harmonics. Analytical expansions are developed for conditions where the surfactant distribution is only slightly perturbed, which occurs when one of the time-scale parameters is small.

---

## 1. Introduction

Surfactants play an important role in the formation and stabilization of emulsions and foams. The non-equilibrium behaviour of these systems, including emulsion rheology and foam drainage, are strongly influenced by the presence of Marangoni stresses (surface tension gradients) that result from surfactants adsorbed at fluid–fluid interfaces. Even trace quantities of surfactants can have a significant qualitative effect as exemplified by the classical work of Levich (1962) on the rise velocity of fine bubbles.

There have been numerous theoretical and numerical investigations on the dynamics of surfactant-covered emulsion drops (Oldroyd 1955; Flumerfelt 1980; Palierne 1990; Stone & Leal 1990; Pawar & Stebe 1996; Li & Pozrikidis 1997; Yon & Pozrikidis 1998; Danov 2001). However, a fundamental understanding of surfactant effects is unavailable because of the complex coupling of drop deformation and surface tension gradients arising from surfactant redistribution.

In an attempt to further a basic understanding of the influence of surfactants on emulsion rheology, we recently developed a theory for the dynamics of a spherical surfactant-covered drop in stationary flows (Bławdziewicz, Vlahovska & Loewenberg 2000, hereafter referred to as I). Drops remain nearly spherical under small-capillary-number conditions, yet significant surfactant redistribution on the interface occurs for low surfactant elasticity (low surface concentration). Effects of surfactant solubility

<sup>†</sup> Present address: Department of Mechanical Engineering, Yale University, New Haven, CT 06520-8286, USA.

were neglected under the assumption that the time scale  $t_{\text{ad}}$  for adsorption/desorption of surfactant on the drop interface is large compared to the inverse shear rate. For dilute surfactant solutions, adsorption is diffusion-controlled with  $t_{\text{ad}} = K^2/D$ , where  $D$  is diffusion coefficient and  $K$  is the adsorption constant. Given  $D \approx 10^{-6} \text{ cm}^2 \text{ s}^{-1}$  and  $K \approx 10^{-2} \text{ cm}$  (e.g. Maldarelli & Huang 1996; Horozov & Arnaudov 2000), surfactant solubility is unimportant for shear rates greater than  $0.01 \text{ s}^{-1}$ . Effects of interfacial viscosity are unimportant for low surface coverage (except possibly for high-molecular-weight surfactants) and were therefore not included in the study. Small-capillary-number conditions, insoluble surfactant, and negligible interfacial viscosity are also assumed in the present paper.

In sufficiently weak flows, the adsorbed surfactant layer is nearly incompressible, because Marangoni stresses equilibrate quickly compared to the inverse shear rate (Bławdziewicz, Cristini & Loewenberg 1999; Bławdziewicz, Wajnryb & Loewenberg 1999). Thus, in a linear flow, an isolated spherical drop covered with insoluble surfactant behaves as a rigid sphere, and the viscosity of a dilute emulsion is given by Einstein's formula. At high shear rates, surfactant is passively convected on the drop interface and the viscosity is given by Taylor's formula. The non-Newtonian rheology at intermediate shear rates, including shear thinning and normal stress differences, was discussed in I.

In the present paper, we explore the dynamics of surfactant-covered spherical drops in time-dependent flows. We show that complex rheology can result from the interplay of the four time scales that are relevant to the problem. These time scales are defined in §2. Our approach, outlined in §3, is based on the theoretical formulation developed in I. Numerical results for the transient and long-time behaviour of surfactant-covered drops in stationary and periodic two-dimensional linear flows are presented in §4 and §5. Analytical solutions are developed, in §6 and §7, for small perturbations of the surfactant distribution. Small perturbations occur for large surfactant elasticity, high-viscosity drops, or high-frequency oscillatory flow.

## 2. Surfactant-covered spherical drops

### 2.1. Assumptions

We consider the nonlinear viscoelastic behaviour of a dilute monodisperse emulsion of surfactant-covered spherical drops with radius  $a$ . Creeping-flow conditions are assumed. The continuous phase has viscosity  $\eta$ , the drops have viscosity  $\lambda\eta$ , and we define  $\hat{\lambda} = \lambda + 1$ . The surfactant forms a dilute film on the drop interface and is insoluble in the bulk phases. Surface diffusion and surface viscosity are negligible.

The emulsion undergoes a two-dimensional linear flow

$$\mathbf{u}_\infty(\mathbf{r}) = \dot{\gamma}(t)\mathbf{E} \cdot \mathbf{r}, \quad (2.1)$$

where

$$\dot{\gamma}(t) = \dot{\gamma}_0 f(t) \quad (2.2)$$

is a time-dependent shear rate with amplitude  $\dot{\gamma}_0$ . The velocity gradient is

$$\mathbf{E} = \frac{1}{2} \begin{pmatrix} 0 & 1 + \beta & 0 \\ 1 - \beta & 0 & 0 \\ 0 & 0 & 0 \end{pmatrix}, \quad (2.3)$$

where  $\beta$  is the magnitude of the vorticity component of the flow;  $\beta = 0$  corresponds to planar extensional flow, and  $\beta = 1$  corresponds to shear flow.

In creeping flows, drops remain spherical provided that the capillary number is small,

$$Ca = \frac{\eta\dot{\gamma}_0 a}{\sigma_{\text{eq}}} \ll 1, \quad (2.4)$$

where  $\sigma_{\text{eq}}$  is the interfacial tension corresponding to the average surfactant concentration. In the zero-capillary-number limit, the nonlinear rheological behaviour of a dilute emulsion results entirely from surfactant redistribution on the drop interface.

## 2.2. Characteristic time scales

The dynamics of surfactant-covered spherical drops is characterized by four time scales. Distortion of the surfactant distribution by the extensional component of the incident flow occurs on the time scale

$$t_d = \hat{\lambda}\dot{\gamma}_0^{-1}, \quad (2.5)$$

and the other three time scales are associated with the mechanisms that control the magnitude of surfactant distortion. Relaxation of the surfactant distribution by Marangoni stresses occurs on the time scale

$$t_\sigma = \frac{\hat{\lambda}\eta a}{\Delta\sigma}, \quad (2.6)$$

where  $\Delta\sigma = \sigma_0 - \sigma_{\text{eq}}$ , and  $\sigma_0$  is the interfacial tension in the absence of surfactant. The extent of surfactant redistribution is also limited by drop rotation, which occurs on the time scale

$$t_r = (\beta\dot{\gamma}_0)^{-1}. \quad (2.7)$$

In oscillatory flows, surfactant redistribution is further limited by flow reversal on the time scale

$$t_\omega = \omega^{-1}, \quad (2.8)$$

where  $\omega$  is the imposed angular frequency.

The strengths of the three mechanisms that limit surfactant redistribution by the flow are characterized by the corresponding time scale ratios: the Marangoni parameter (inverse Marangoni number)

$$Ma^{-1} = \frac{t_\sigma}{t_d}, \quad (2.9)$$

the rotation parameter

$$\hat{\beta}^{-1} = \frac{t_r}{t_d} = (\beta\hat{\lambda})^{-1}, \quad (2.10)$$

and the frequency parameter

$$\bar{\omega}^{-1} = \frac{t_\omega}{t_d}. \quad (2.11)$$

The smallest of these parameters controls the magnitude of surfactant redistribution. In this paper, we explore the complex drop dynamics that results from the nonlinear interaction of the time scales present in the problem.

## 2.3. Surfactant transport

Hereafter we use dimensionless variables with length scaled by  $a$ , time by  $\dot{\gamma}_0^{-1}$ , bulk stresses by  $\eta\dot{\gamma}_0$ , and interfacial tension by  $\eta\dot{\gamma}_0 a$ . The surfactant concentration  $\Gamma$  is normalized by the average surfactant concentration  $\Gamma_{\text{eq}}$ .

The evolution of an insoluble, non-diffusing surfactant is governed by the interfacial continuity equation

$$\frac{\partial \Gamma}{\partial t} + \nabla_s \cdot (\Gamma \mathbf{u}_s) = 0, \quad (2.12)$$

where  $\nabla_s$  denotes the surface gradient operator,  $\mathbf{u}_s$  is the interfacial velocity, and the coordinate system is centred at the drop.

The ratio of the time scale for surface diffusion of surfactant  $t_{sd} = a^2/D_s$  to the Marangoni relaxation time (2.6) is  $t_{sd}/t_\sigma \simeq ab\Delta\sigma/k_B T$ , where  $D_s \simeq k_B T/\eta b$  is the surface diffusion coefficient for surfactant molecules with hydrodynamic radius  $b$ . Given that  $\Delta\sigma \approx k_B T \Gamma_{eq}$  and  $\Gamma_{eq} \sim b^{-2}$ , the time-scale ratio is  $t_{sd}/t_\sigma \sim a/b$ . Since  $a \gg b$ , the time scale for surface diffusion is much longer than the relevant time scales of the problem. Surface diffusion is therefore unimportant and is neglected in (2.12).

Under creeping-flow conditions the instantaneous fluid motion on both sides of the interface is described by the Stokes equations,

$$\bar{\eta}_i \nabla^2 \mathbf{u} - \nabla p = 0, \quad \nabla \cdot \mathbf{u} = 0 \quad (2.13)$$

(with  $i = 1, 2$ ), where the dimensionless viscosity of the outside fluid is  $\bar{\eta}_1 = 1$  and the inside fluid is  $\bar{\eta}_2 = \lambda$ . The velocity field is continuous, and the normal velocity component vanishes at the interface (spherical drops). At infinity the flow tends to the incident flow (2.1). The discontinuity of the tangential traction across the interface is balanced by the gradient of surface tension,

$$\mathbf{I}_s \cdot (\boldsymbol{\tau}_{out} - \boldsymbol{\tau}_{in}) \cdot \hat{\mathbf{r}} = -\nabla_s \sigma, \quad (2.14)$$

where  $\hat{\mathbf{r}} = \mathbf{r}/r$  is the unit normal vector, and  $\mathbf{I}_s = \mathbf{I} - \hat{\mathbf{r}}\hat{\mathbf{r}}$  is the surface projection operator.

Herein we focus on spherical drops with significant surfactant redistribution on their interfaces, i.e.  $Ma = O(1)$ ,  $Ca \ll 1$ . Equations (2.4) and (2.9) thus imply that  $\Delta\sigma/\sigma_{eq} \ll 1$ , so a linear interfacial equation of state is used

$$\sigma(\Gamma) = \sigma(1) - Ma \bar{\Gamma}, \quad (2.15)$$

where  $\bar{\Gamma}$  is the deviation of the surfactant concentration from the equilibrium value,

$$\Gamma = 1 + \bar{\Gamma}. \quad (2.16)$$

#### 2.4. Effective rheological properties

In a linear flow (2.1), the traceless part of the average stress tensor has the form

$$\Sigma = 2\mathbf{E}^s + \phi \boldsymbol{\tau}^d, \quad (2.17)$$

where  $\mathbf{E}^s$  denotes the symmetric part of  $\mathbf{E}$ ,  $\boldsymbol{\tau}^d$  is the drop contribution to the stress, and  $\phi$  is the drop volume fraction. In a dilute emulsion  $\boldsymbol{\tau}^d$  can be obtained from the solution of a Stokes-flow problem for an isolated drop.

In a two-dimensional linear flow (2.3),  $\boldsymbol{\tau}^d$  is fully characterized by the shear stress  $\tau_{12}^d$  and two normal stress differences  $N_1$  and  $N_2$ . By the linearity of the Stokes equations, the stress tensor has the form

$$\tau_{12}^d = \tau_{12}^0 + \tau_{12}^f, \quad (2.18)$$

where

$$\tau_{12}^0 = \frac{\zeta}{2} - \frac{3}{2} \hat{\lambda}^{-1} \quad (2.19)$$

is the contribution corresponding to a drop with a surfactant-free interface (Taylor

1932), and  $\tau_{12}^F$  is the extra stress contribution resulting from Marangoni stresses. The first and second normal stress differences

$$N_1 = \tau_{11}^F - \tau_{22}^F, \quad N_2 = \tau_{22}^F - \tau_{33}^F \quad (2.20)$$

result solely from Marangoni stresses.

In stationary flows with small shear rates, the emulsion behaves as a suspension of rigid spheres, with  $\tau_{12}^d = \frac{5}{2}$ ; at high shear rates the shear stress is equal to the clean-drop value (2.19). The maximum decrease of the shear stress in stationary flows is thus

$$\tau_{\max} = \frac{3}{2} \hat{\lambda}^{-1}. \quad (2.21)$$

### 3. Evolution equations

#### 3.1. Matrix representation

In I, the evolution equations (2.12)–(2.15) were transformed into a matrix representation. According to this procedure, the surfactant distribution is expanded in spherical harmonics (Edmonds 1960),

$$\bar{\Gamma} = \sum_{l=2}^{\infty} \sum_{m=-l}^l \gamma_{lm}(t) Y_{lm}(\theta, \phi), \quad (3.1)$$

where  $\theta$  and  $\phi$  are the polar and azimuthal angles. The summation is over even values of  $l$  and  $m$  on the assumption that the perturbation of surfactant distribution results entirely from the imposed linear flow (2.1). The boundary-value problem (2.13)–(2.15) is then solved by expansion into appropriate sets of fundamental solutions, and the result is inserted into the conservation equation (2.12) to obtain an evolution equation of the form

$$\begin{aligned} \frac{\partial \gamma_{lm}}{\partial t} = f(t) [\hat{\lambda}^{-1} C_{lm} + \frac{1}{2} i m \beta \gamma_{lm} + \hat{\lambda}^{-1} A_{lm'l'm'}] \\ + \hat{\lambda}^{-1} Ma [W(l) \gamma_{lm} + \Theta_{lm'l'm''} \gamma_{l'm''}], \end{aligned} \quad (3.2)$$

where  $i^2 = -1$ . Summation over repeated indices is implied. The above equation is equivalent to equation (81) in I, except that the vorticity parameter  $\beta$  and time-dependent flow amplitude  $f(t)$  have been introduced.

In equation (3.2), the terms proportional to  $f(t)$  represent convection of the surfactant by the imposed flow. The rigid-body rotation of the drop by the vorticity component of the flow is described by  $\frac{1}{2} i m \beta \gamma_{lm}$ , and the terms that scale with  $\hat{\lambda}^{-1}$  represent surfactant redistribution by the straining component of the flow. The inhomogeneous term

$$C_{lm} = \mp i (\frac{6}{5} \pi)^{1/2} \delta_{l2} \delta_{m\pm 2} \quad (3.3)$$

corresponds to the uniform contribution in (2.16). The matrix  $A$  corresponds to convection of the non-uniform contribution  $\bar{\Gamma}$ ; the matrix elements are given in Appendix A.

The terms proportional to  $Ma$  in equation (3.2) describe the relaxation of the surfactant distribution by Marangoni stresses. The coefficient of the linear term is

$$W(l) = -\frac{l(l+1)}{2l+1}, \quad (3.4)$$

and the matrix  $\Theta$  is defined in Appendix A.

The shear and normal stresses are directly related to the surfactant distribution coefficients,

$$\tau_{12}^r = ic_0 \hat{\lambda}^{-1} Ma (\gamma_{22} - \gamma_{2-2}), \quad (3.5)$$

and

$$N_1 = 2c_0 \hat{\lambda}^{-1} Ma (\gamma_{22} + \gamma_{2-2}), \quad (3.6)$$

$$N_2 = -\frac{1}{2} N_1 - c_0 \sqrt{6} \hat{\lambda}^{-1} Ma \gamma_{20}, \quad (3.7)$$

where

$$c_0 = \left( \frac{27}{40\pi} \right)^{1/2}. \quad (3.8)$$

Relations (3.5)–(3.7) are obtained from equations (64)–(66) in I, by combining them with the results in Appendix C of I.

### 3.2. Scale transformation for linear flows with different vorticity

The rate of distortion and Marangoni relaxation of the surfactant distribution is proportional to the viscosity parameter  $\hat{\lambda}^{-1}$  according to equation (3.2), while the angular velocity of the surfactant distribution  $\frac{1}{2}\beta$  by the vorticity component of the imposed flow is independent of the viscosity ratio. Thus, the relative effect of drop rotation on surfactant evolution is characterized by the combined parameter  $\hat{\beta}$  (equation (2.10)), rather than  $\hat{\lambda}$  and  $\beta$  separately. This is seen by dividing both sides of equation (3.2) by  $\beta$ , and rescaling time

$$t' = \beta t. \quad (3.9)$$

For spherical drops the invariance of the evolution with respect to the above scaling transformation is exact. For deformable drops the transformation holds in the asymptotic regime  $\hat{\lambda} \gg 1$ , but in general the dynamics has a more complicated dependence on viscosity ratio (Rallison 1980). A related dynamical similarity also applies to the motion of Brownian axisymmetric rigid particles in linear flows, where the combined rotation parameter is given by the product of  $\beta^{-1}$  and the rotational mobility in straining flow (Rao, Tang & Altan 1994; Szeri & Lin 1996).

In what follows, we restrict our discussion to the behaviour of drops in shear flow, thus  $\hat{\beta} = \hat{\lambda}$ . However, since the response of the system is fully characterized by the parameters  $Ma^{-1}$ ,  $\hat{\beta}^{-1}$ , and the time dependence of the imposed flow  $f(t')$ , the corresponding results for (non-zero)  $\beta \neq 1$  are obtained by transformation (3.9), and the substitution

$$\hat{\lambda} \rightarrow \hat{\beta}. \quad (3.10)$$

Note that for oscillatory flows, relations (2.11) and (3.9) yield  $\bar{\omega} = \omega \hat{\beta}$ , assuming that  $\omega^{-1}$  is scaled as  $t'$ .

### 3.3. Solution of evolution equations

The infinite array of surfactant evolution equations (3.2) was solved numerically, with the truncation  $\gamma_{lm} = 0$  for  $l > l_{\max}$ . The results presented in this paper were obtained using  $l_{\max} = 8$ , and the accuracy was verified using higher-order truncations. The frequency response was evaluated by Fourier transform of the numerical solution.

For conditions where one of the time-scale parameters (2.9)–(2.11) is small, perturbation expansions were derived.

#### 4. Stress evolution upon inception of steady shear flow

Here we consider an initially quiescent emulsion subjected to an impulsively started shear flow

$$f(t) = \begin{cases} 0, & t < 0 \\ 1, & t \geq 0. \end{cases} \quad (4.1)$$

The evolution of shear stress  $\tau_{12}^F$  and normal stress differences  $N_1$  and  $N_2$  is shown in figures 1 and 2 for different values of the Marangoni parameter. The value of the viscosity/rotation parameter (2.10) is  $\hat{\lambda}^{-1} = \frac{1}{2}$ , thus  $t_r \simeq t_d$ . The results show that the system approaches steady state on the surfactant-relaxation time scale  $t_\sigma$  and exhibits decaying oscillations with frequency  $t_r^{-1}$ . Similar behavior occurs for smaller values of  $\hat{\lambda}^{-1}$  ( $t_r < t_d$ ), except that the amplitude of the response is smaller, because the surfactant distribution deforms more slowly, while drop rotation is unaffected by the drop viscosity.

Similar numerical calculations show that upon cessation of steady shear flow stresses relax monotonically in all cases.

#### 5. Stress response in oscillatory flow

In this section, we consider the response of the emulsion in an oscillatory shear flow (2.1) with

$$f(t) = \cos \omega t. \quad (5.1)$$

##### 5.1. Dependence on flow frequency

In figure 3, surfactant contribution to the shear stress is shown as a function of time and as a function of strain (Lissajous figures) in flows with different frequencies. The system parameters are  $Ma^{-1} = 1$  and  $\hat{\lambda}^{-1} = \frac{1}{2}$ , which corresponds to  $t_\sigma \simeq t_r \simeq t_d$ . The time dependence of the stress is presented for the long-time periodic response; the transient relaxation (on time scale  $t_\sigma$ ) is shown only in the stress-strain plots. At long times, the shear stress oscillates about a zero mean value, with the externally imposed period  $T = 2\pi/\omega$ . By contrast, the first and second normal stress differences, shown in figure 4, have non-zero mean values and period  $\frac{1}{2}T$  as a result of the invariance with respect to flow reversal.

##### 5.1.1. Quasi-static response

Conditions in figures 3(a) and 4(a) correspond to very low frequencies,  $t_\omega \gg t_\sigma$ . Under these conditions, the long-time response of the system is quasi-static,

$$\boldsymbol{\tau}^F(t) = \boldsymbol{\tau}_{\text{stat}}^F[\dot{\gamma}(t)], \quad (5.2)$$

where  $\boldsymbol{\tau}_{\text{stat}}^F$  is the stationary stress in a steady flow with shear rate  $\dot{\gamma}(t)$  ( $\boldsymbol{\tau}^F$  and  $\boldsymbol{\tau}_{\text{stat}}^F$  are normalized by  $\eta\dot{\gamma}_0$ ). The shapes of the low-frequency stress-response curves stem from the alignment of the stationary surfactant distribution with the flow at high shear rates, as required by the symmetry of Stokes equations with respect to flow reversal. As explained in I, an aligned surfactant distribution contributes to the normal stresses but not the shear stress. Thus,  $N_1$  and  $N_2$  tend to constant values at high shear rates, whereas the shear stress decreases as  $\tau_{12} \sim \dot{\gamma}^{-1}$ . It follows that in the low-frequency quasi-static regime, the normal stresses vary slowly in the high-shear-rate portion of the flow cycle, and the shear stress passes through a maximum as  $\dot{\gamma}$  increases, producing the dimpled shape of the response function.

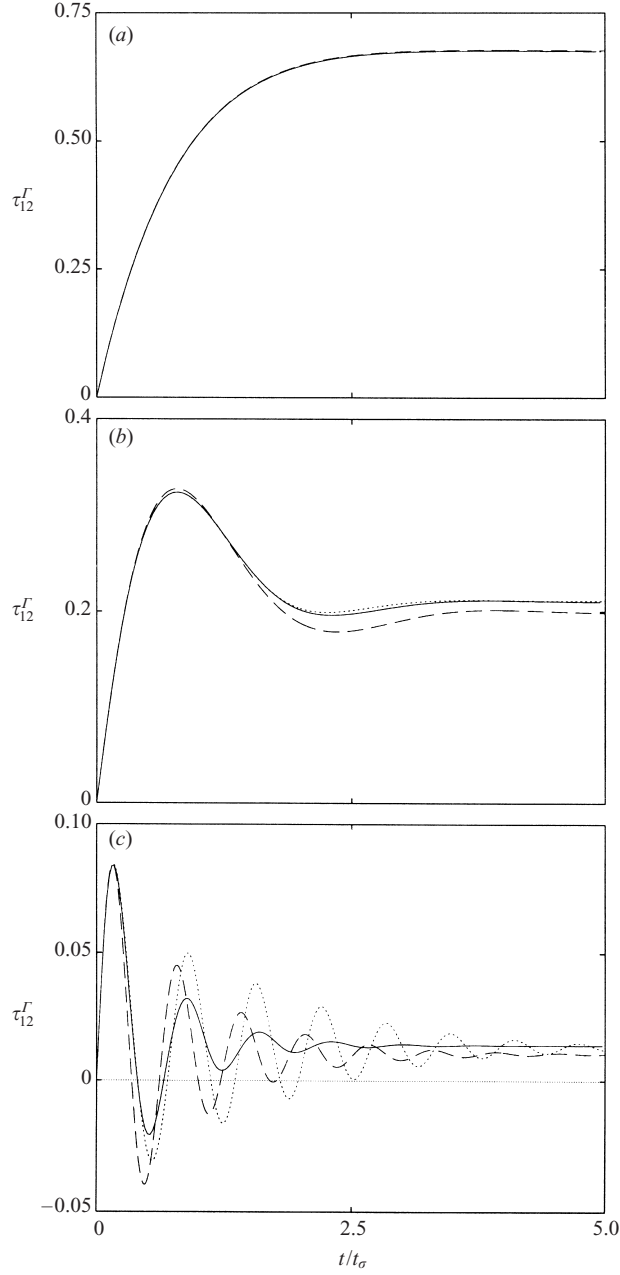


FIGURE 1. Shear-stress evolution after inception of steady shear flow, versus time normalized by surfactant relaxation time;  $\hat{\lambda}^{-1} = \frac{1}{2}$ , Marangoni parameter  $Ma^{-1} = (a)$  0.2,  $(b)$  1,  $(c)$  5. Numerical integration of equation (3.2) (solid line); corotational expansion (6.8) truncated at  $O(\hat{\lambda}^{-1})$  (dashed line) and  $O(\hat{\lambda}^{-3})$  (dotted line).

### 5.1.2. Nonlinear viscoelastic response

Figures 3(b–e) and 4(b–c) illustrate the change in the rheological response of surfactant-covered drops when the frequency parameter (2.11) is decreased. The results indicate that the shear-stress response becomes asymmetric with decreasing  $\bar{\omega}^{-1}$ , and

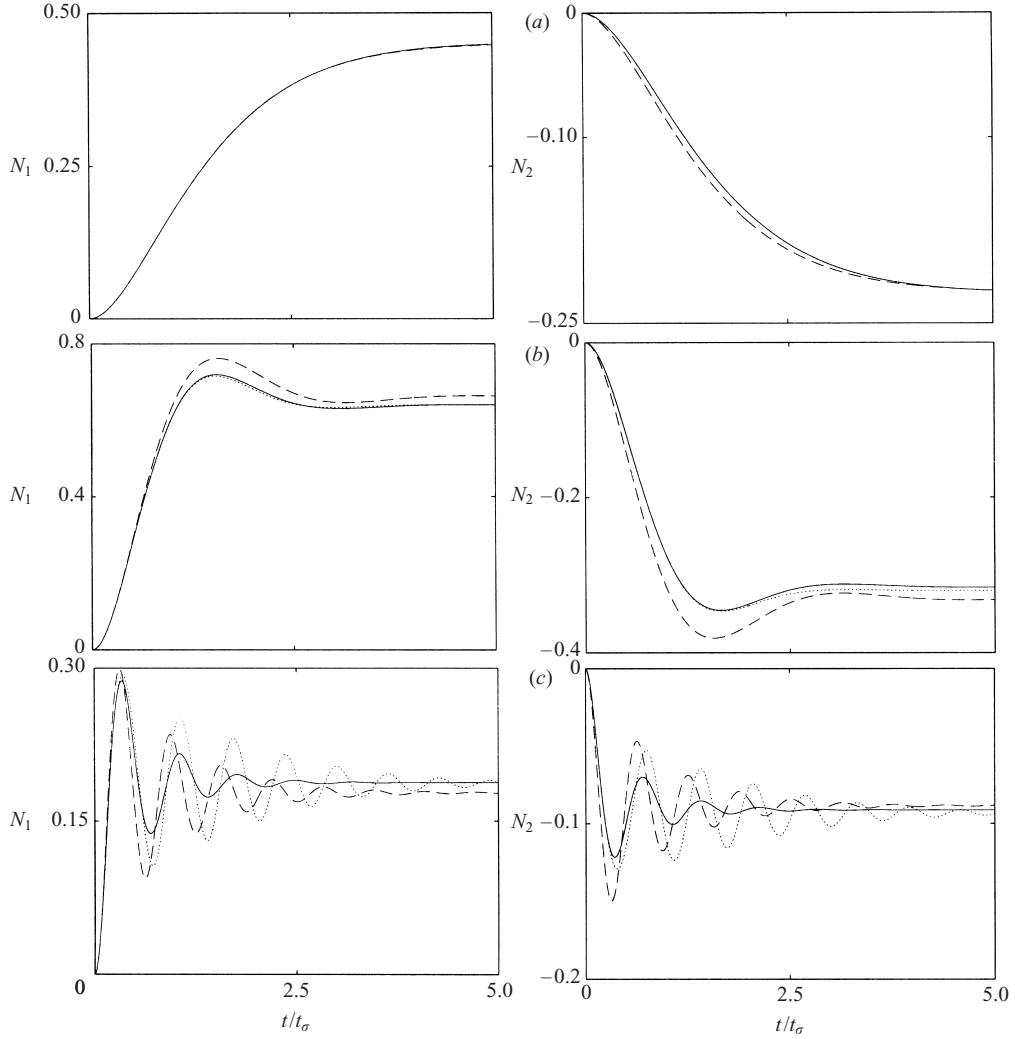


FIGURE 2. Same as figure 1, but for normal stress differences, and with corotational expansion (6.9)–(6.10).

a phase shift occurs with respect to  $\dot{\gamma}(t)$ . At high frequencies,  $\bar{\omega}^{-1} \ll 1$ , the response of the system becomes linear, because the strain amplitude, and thus the perturbation of the surfactant distribution, remain small. The response is predominantly elastic in this regime, i.e. in phase with the strain. There is no linear contribution to normal stresses, thus  $N_1$  and  $N_2$  are small in the high-frequency regime, as seen in figure 4(c).

### 5.1.3. Fourier decomposition

In the long-time periodic regime, the shear stress and the normal stresses can be decomposed into Fourier modes,

$$\tau_{12}^r = \sum_{k=1}^{\infty} [\eta_k' \cos(k\omega t) + \eta_k'' \sin(k\omega t)] \quad (5.3)$$

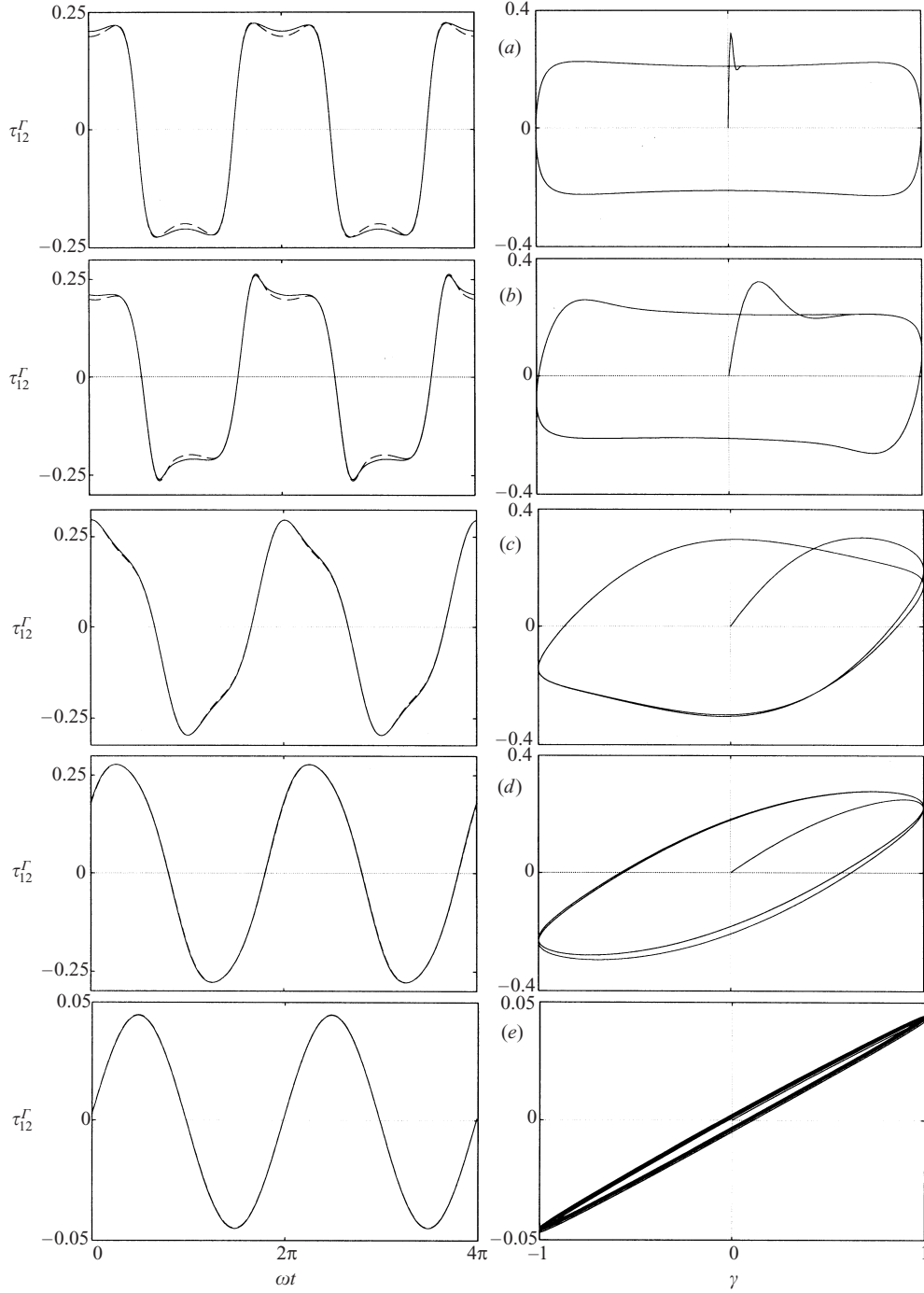


FIGURE 3. Shear-stress response in oscillatory flow, versus time and strain;  $Ma^{-1} = 1$ ,  $\hat{\lambda}^{-1} = \frac{1}{2}$ , frequency parameter  $\bar{\omega}^{-1} =$  (a) 50, (b) 10, (c) 0.5, (d) 0.1, (e) 0.05. Numerical integration of equation (3.2) (solid line); corotational expansion (6.8) truncated at  $O(\hat{\lambda}^{-1})$  (dashed line). For  $\bar{\omega}^{-1} \leq 0.5$ , the curves corresponding to the expansion and numerical integration are indistinguishable; for  $\bar{\omega}^{-1} = 50$ , the quasi-static result (5.2) coincides with the numerical results.

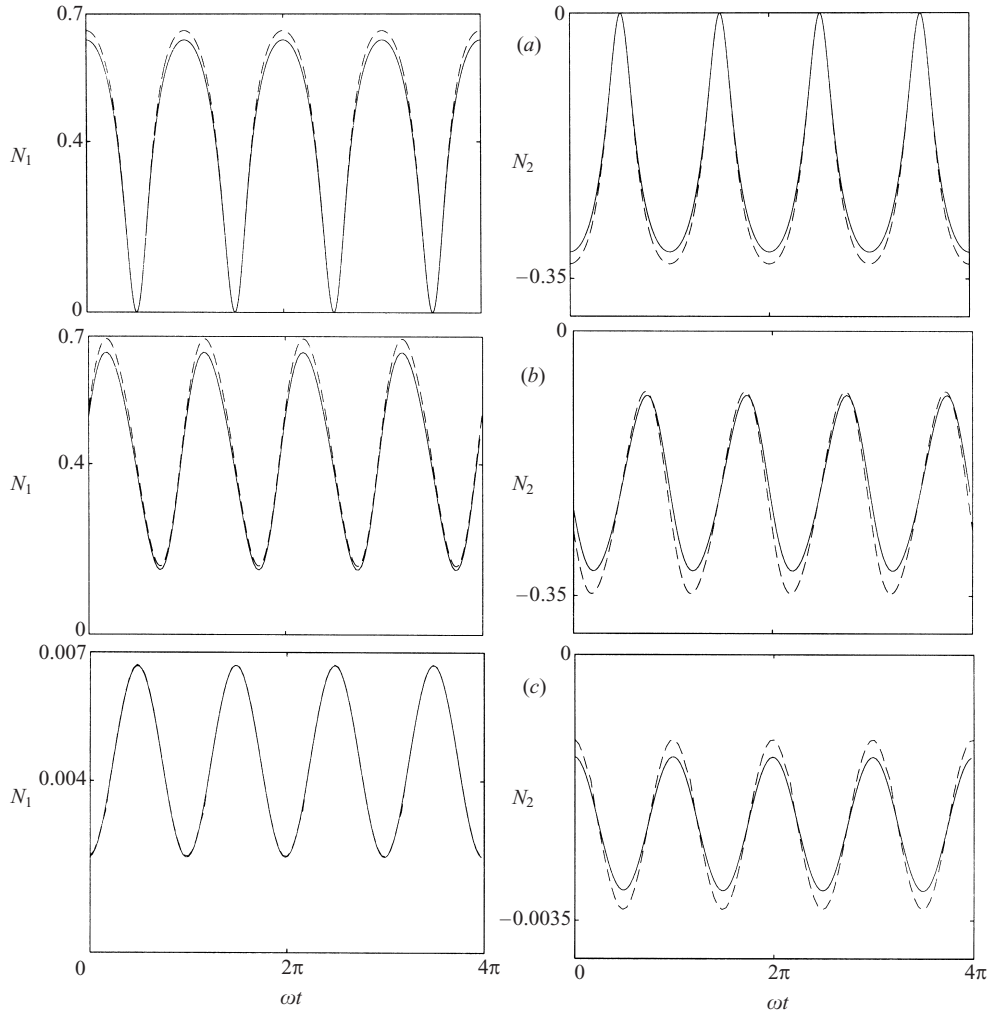


FIGURE 4. Same as figure 3, but for normal stress differences and  $\bar{\omega}^1 = (a) 50, (b) 0.5, (c) 0.05$ , and with corotational expansion (6.9)–(6.10).

and

$$N_i = N'_{i,0} + \sum_{k=2}^{\infty} [N'_{i,k} \cos(k\omega t) + N''_{i,k} \sin(k\omega t)], \quad (5.4)$$

where  $i = 1, 2$ . The summation in equation (5.3) is over odd  $k$  and in equation (5.4) over even  $k$  as a result of the flow-reversal symmetry.

Several low-order Fourier modes are shown in figure 5 for the shear stress, and in figure 6 for normal stresses. In the linear viscoelastic regime ( $t_\omega \ll t_d$ ), only the fundamental shear-stress mode  $k = 1$  is non-zero, and the response is nearly elastic (i.e.  $\eta''_1 \gg \eta'_1$ ), consistently with the results shown in figures 3(e) and 4(c). With the decreasing frequency, higher-order modes become important. In the low-frequency quasi-static regime the Fourier modes tend to constant values, and  $\eta' \gg \eta''$ .

### 5.2. Effects of drop viscosity

Increasing the drop viscosity lengthens the time scales for surfactant redistribution and relaxation but not the time scale for drop rotation. Drop rotation provides a

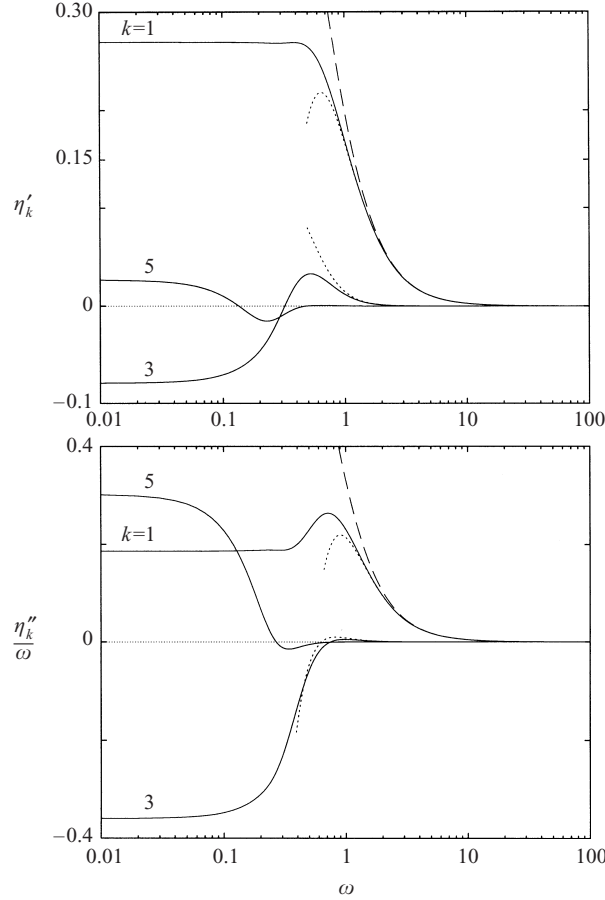


FIGURE 5. Nonlinear shear-stress response functions for modes  $k \leq 5$ ;  $Ma^{-1} = 1$ ,  $\hat{\lambda}^{-1} = \frac{1}{2}$ . Numerical solution (solid line); high Marangoni/frequency expansion (7.10)–(7.11) truncated at  $\tilde{O}(1)$  (dashed line) and  $O(Ma^{-2})$  (dotted line).

restoring mechanism, thus the deformation of the surfactant distribution decreases with  $\hat{\lambda}$ , as seen in figure 7.

If the drop rotation time is the shortest time scale in the problem, decaying oscillations occur during each cycle of the imposed flow, as shown in figures 7 and 8. For  $t_\sigma/t_\omega \equiv \bar{\omega}/Ma \ll 1$ , the response of the system becomes quasi-static by the end of each period, as in figure 8(a), where  $t_\sigma/t_\omega = 0.2$ ; the conditions in figure 8(b,c) correspond to  $t_\sigma/t_\omega = 1$  and  $t_\sigma/t_\omega = 2$ . The oscillations associated with drop rotation are excited at the start of each cycle by the instability of the near-quasi-static surfactant distribution upon flow reversal.

## 6. Corotational expansions

If either the rotational parameter (2.10) or the Marangoni parameter (2.9) is small, equation (3.2) can be solved by perturbation in  $\hat{\lambda}^{-1}$  or  $Ma^{-1}$  with

$$\tilde{Ma} = \frac{Ma}{\hat{\lambda}} = t_r/t_\sigma \quad (6.1)$$

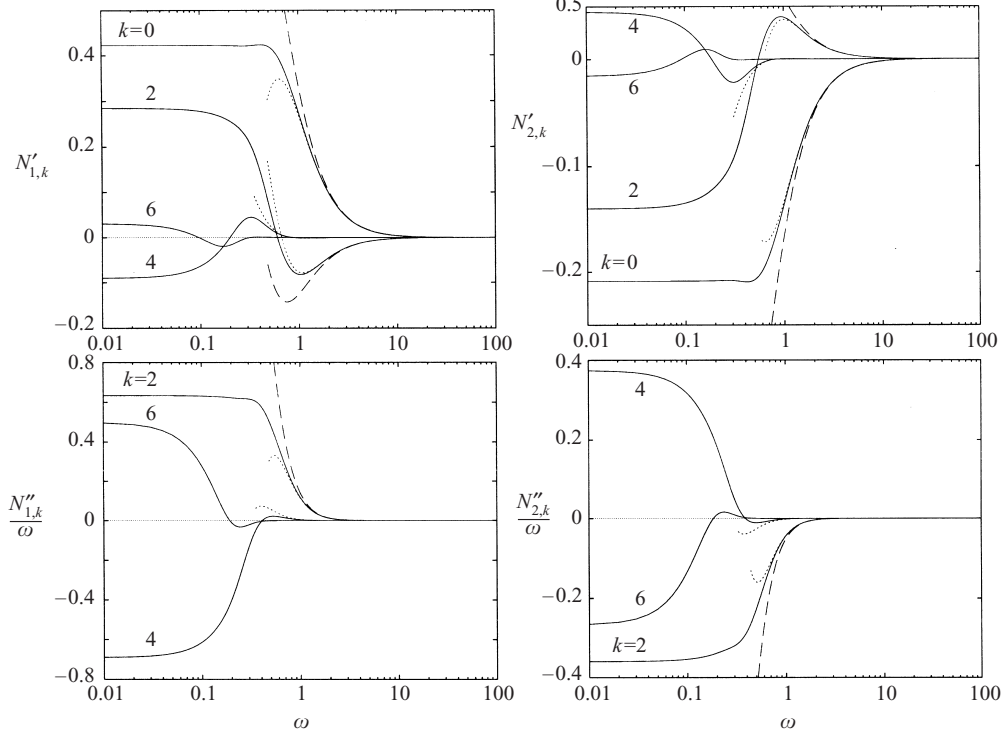


FIGURE 6. Same as figure 5, but for normal stress differences and  $k \leq 6$ . The corresponding high Marangoni/frequency expansion (7.12)–(7.13) truncated at  $O(Ma^{-1})$  (dashed line) and  $O(Ma^{-3})$  (dotted line).

fixed. The resulting expansions

$$\gamma_{lm} = \sum_{p=1}^{\infty} \hat{\lambda}^{-p} \gamma_{lm}^{(p)}(\tilde{M}a) \quad (6.2)$$

and

$$\gamma_{lm} = \sum_{p=1}^{\infty} Ma^{-p} \tilde{\gamma}_{lm}^{(p)}(\tilde{M}a) \quad (6.3)$$

are related by

$$\tilde{\gamma}_{lm}^{(p)}(\tilde{M}a) = \tilde{M}a^p \gamma_{lm}^{(p)}(\tilde{M}a). \quad (6.4)$$

The expansion coefficients  $\gamma_{lm}^{(p)}$  satisfy the perturbation equations

$$\frac{\partial \gamma_{lm}^{(1)}}{\partial t} - [\tilde{M}a W(l) + \frac{1}{2} imf(t)] \gamma_{lm}^{(1)} = \mp c_0 f(t) \delta_{l2} \delta_{m\pm 2} \quad (6.5)$$

and

$$\begin{aligned} \frac{\partial \gamma_{lm}^{(p+1)}}{\partial t} - [\tilde{M}a W(l) + \frac{1}{2} imf(t)] \gamma_{lm}^{(p+1)} \\ = f(t) A_{lm'l'm'} \gamma_{l'm'}^{(p)} + \Theta_{lm'l'm''} \sum_{j=0}^p \gamma_{l''m''}^{(j)} \gamma_{l'm'}^{(p-j)}, \end{aligned} \quad (6.6)$$

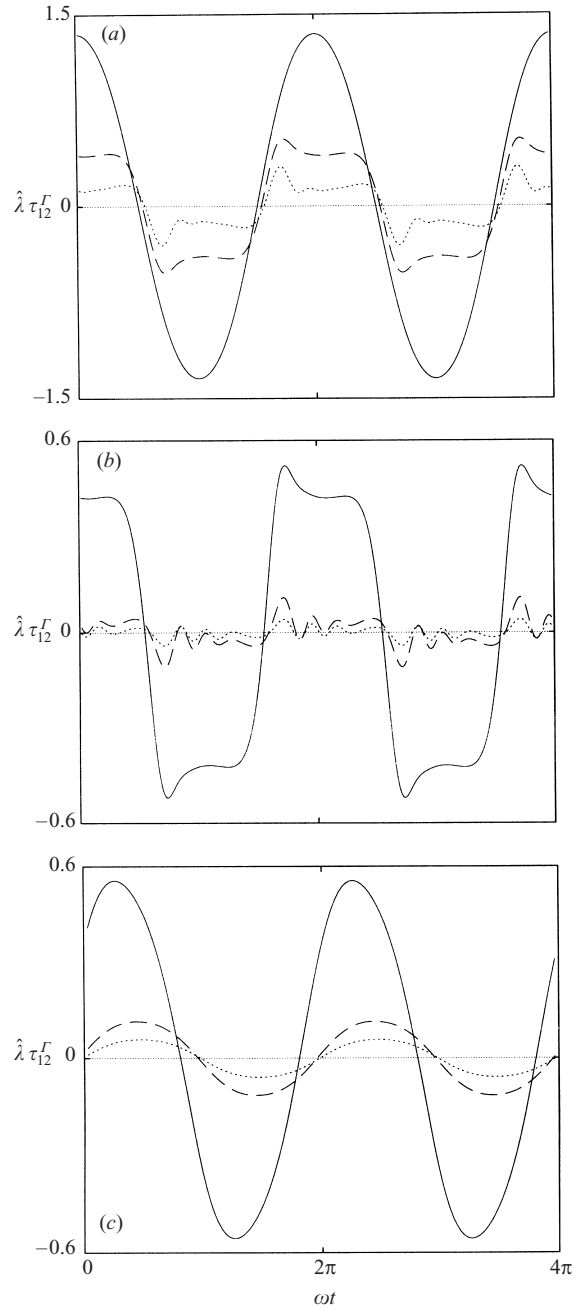


FIGURE 7. Long-time periodic response of shear-stress in oscillatory flow for  $\hat{\lambda}^{-1} = \frac{1}{2}$  (solid line),  $\hat{\lambda}^{-1} = 0.1$  (dashed line), and  $\hat{\lambda}^{-1} = 0.05$  (dotted line). Marangoni parameter and frequency: (a)  $Ma^{-1} = 0.2$ ,  $\omega = 0.1$ ; (b)  $Ma^{-1} = 1$ ,  $\omega = 0.1$ ; (c)  $Ma^{-1} = 1$ ,  $\omega = 1$ .

where  $p = 1, 2, \dots$ . The triangle condition (A 6) implies that the coupling of harmonics with orders  $l'$  and  $l''$  produces only harmonics of orders  $l \leq l' + l''$ . Thus, assuming an initially uniform surfactant distribution, equation (6.6) yields

$$\gamma_{lm}^{(p)} = 0 \quad \text{for } l > 2p, \quad (6.7)$$

and only finite matrices are therefore involved at each order.

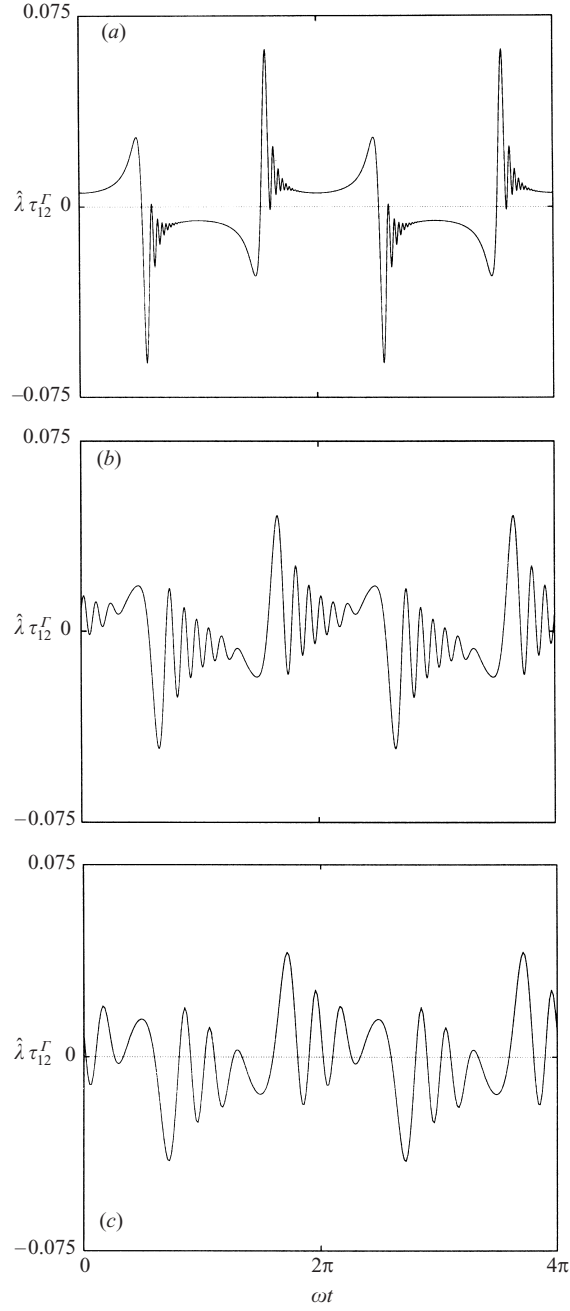


FIGURE 8. Long-time shear-stress response for high-viscosity drops in oscillatory flow;  $\hat{\lambda}^{-1} = 0.1$ ,  $Ma^{-1} = 2$ . Frequency parameter  $\bar{\omega}^{-1} = (a) 10$ ,  $(b) 2$ ,  $(c) 1$ . Numerical results and corotational expansion (6.8) coincide.

An inspection of equations (3.2) and (6.5)–(6.6) reveals that the expansion coefficients  $\gamma_{lm}^{(p)}(\tilde{Ma})$  and  $\tilde{\gamma}_{lm}^{(p)}(\tilde{Ma})$  are bounded in the region  $0 \leq \tilde{Ma} < \infty$ . Accordingly, the expansions (6.2) and (6.3) converge uniformly for  $\hat{\lambda}^{-1} \ll 1$  or for  $Ma^{-1} \ll 1$ .

High-viscosity expansions for the stress components,

$$\tau_{12}^r = \sum_{k=0}^{\infty} \hat{\lambda}^{-(2k+1)} \tau_{12}^{(2k+1)}, \quad (6.8)$$

$$N_1 = \sum_{k=0}^{\infty} \hat{\lambda}^{-(2k+1)} N_1^{(2k+1)}, \quad (6.9)$$

$$N_2 = -\frac{1}{2} N_1 + \sum_{k=1}^{\infty} \hat{\lambda}^{-2k} N_2^{(2k)}, \quad (6.10)$$

are obtained by inserting (6.2) into (3.5)–(3.7). Only odd powers of  $\hat{\lambda}^{-1}$  contribute to the shear stress and the first normal stress difference  $N_1$ ; the second normal stress difference  $N_2$  depends on both odd and even powers of  $\hat{\lambda}^{-1}$ . The corresponding expansions in  $Ma^{-1}$  are obtained using relation (6.4).

Expansions (6.8)–(6.10) are corotational (i.e. preserve invariance with respect to transformation to a rotating coordinate system), because in the perturbation equations (6.5) and (6.6) the time derivative and rotation operator  $\frac{1}{2}im$  appear at same order. Moreover, the leading-order perturbation equation (6.5) is linear and involves only second-order harmonics. This implies that the leading-order terms in the expansions (6.8)–(6.10) are equivalent to the corotational Maxwell model (Bird, Armstrong & Hassager 1977).

### 6.1. Inception of steady shear flow

For the start-up problem (4.1), perturbation equations (6.5)–(6.6) can be integrated explicitly. At the leading order we obtain

$$\tau_{12}^{(1)}(t) = \tau_{12}^{(1),\text{stat}} \{1 - \exp(-t/t_0)[\cos(t) - t_0 \sin(t)]\}, \quad (6.11)$$

$$N_1^{(1)}(t) = N_1^{(1),\text{stat}} \{1 - \exp(-t/t_0)[\cos(t) + \frac{1}{t_0} \sin(t)]\}, \quad (6.12)$$

$$N_2^{(1)}(t) = -\frac{1}{2} N_1^{(1)}(t), \quad (6.13)$$

where

$$\tau_{12}^{(1),\text{stat}} = \frac{3}{2} \frac{1}{1 + t_0^2}, \quad (6.14)$$

$$N_1^{(1),\text{stat}} = -2N_2^{(1),\text{stat}} = \frac{3t_0}{1 + t_0^2} \quad (6.15)$$

are the stationary contributions at long times, and

$$t_0 = \frac{5}{6\overline{Ma}} \quad (6.16)$$

is the relaxation time. The above results are equivalent to the corotational Maxwell model with relaxation time  $t_0$ . Relation (6.13) follows from the absence of harmonics with  $m = 0$  in the leading-order equation (6.5).

The integration at the next perturbation level yields

$$N_2^{(2)}(t) = \frac{9}{14} \frac{1}{1 + t_0^2} \left\{ t_0 \exp(-2t/t_0) + \exp\left(-\frac{t}{t_0}\right) [-t_0 \cos(t) + \sin(t)] \right\}. \quad (6.17)$$

The higher-order terms are cumbersome; the  $O(\hat{\lambda}^{-3})$  formulas are listed in Appendix B.

## 6.2. Oscillatory flow

In oscillatory flow (5.1), integration of the leading-order equation (6.5) for the corotational high-viscosity expansion yields

$$\hat{\lambda}\tau_{12}^I(t) = \frac{3}{2}t_0^{-2}I_1(t), \quad (6.18)$$

$$\hat{\lambda}N_1(t) = 3t_0^{-1}[1 - t_0^{-1}I_2(t)], \quad (6.19)$$

$$N_2(t) = -\frac{1}{2}N_1(t), \quad (6.20)$$

where (3.5)–(3.7) have been used, and

$$I_1(t) = \int_0^t \exp(-t'/t_0) \sin \left\{ \frac{1}{\omega} [\sin(\omega t) - \sin \omega(t-t')] \right\} dt', \quad (6.21)$$

$$I_2(t) = \int_0^t \exp(-t'/t_0) \cos \left\{ \frac{1}{\omega} [\sin(\omega t) - \sin \omega(t-t')] \right\} dt'. \quad (6.22)$$

Analytical evaluation of higher-order terms was not possible.

The long-time  $t/t_0 \gg 1$  periodic response of the system is obtained by setting the upper limit in integrals (6.21) and (6.22) to infinity. In the quasi-static regime,  $\omega t_0 \ll 1$ , the integrals (6.21) and (6.22) can be evaluated by expanding the  $\{\}$  terms of the integrands in powers of  $\omega t'$ , which yields

$$I_1^{(0)} = \frac{t_0^2 \cos(\omega t)}{1 + t_0^2 \cos^2(\omega t)} + O(\omega t_0), \quad (6.23)$$

$$I_2^{(0)} = \frac{t_0}{1 + t_0^2 \cos^2(\omega t)} + O(\omega t_0). \quad (6.24)$$

The resulting series has a small convergence radius because the expansions of the integrands are not uniformly valid.

## 6.3. Comparison with numerical results

The corotational high-viscosity expansion is compared to numerical results for the transient start-up problem in figures 1, 2 and for a drop in oscillatory flow in figures 3, 4 and 8. The results in figures 1–4 indicate that the expansion converges rapidly even for moderate-viscosity drops ( $\hat{\lambda}^{-1} = \frac{1}{2}$ ). For the start-up problem (figure 1), several leading-order terms are sufficient to accurately predict stationary values of the stress over the whole range of the Marangoni parameter, as in I; however, the decay rate of the oscillations for  $Ma^{-1} > 1$  is under-predicted (figure 1c). For high-viscosity drops, the exact and approximate results are indistinguishable, as seen in figure 8.

## 7. Expansions of Fourier modes

In the long-time periodic regime for a drop in oscillatory flow, equation (3.2) can be Fourier transformed to yield the hierarchy of equations

$$ik\tilde{\omega}\bar{\gamma}_{lm,k} = \frac{1}{2}C_{lm}(\delta_{-1k} + \delta_{1k}) + W(l)\bar{\gamma}_{lm,k} + Ma^{-1} \left[ \frac{1}{4}im\hat{\lambda}(\bar{\gamma}_{lm,k-1} + \bar{\gamma}_{lm,k+1}) + \frac{1}{2}A_{lm'l''m''}(\bar{\gamma}_{l''m'',k-1} + \bar{\gamma}_{l''m'',k+1}) + \Theta_{lm'l''m''} \sum_{s=-\infty}^{+\infty} \bar{\gamma}_{l''m'',k-s}\bar{\gamma}_{l'm',s} \right], \quad (7.1)$$

for the complex Fourier modes

$$\gamma_{lm} = \sum_{k=-\infty}^{\infty} \gamma_{lm,k} e^{ik\omega t}, \quad (7.2)$$

where  $\gamma_{lm,k} = Ma^{-1} \bar{\gamma}_{lm,k}$ , and  $\gamma_{lm,-k}$  is the complex conjugate of  $\gamma_{lm,k}$ . The parameter  $\tilde{\omega}$  is defined by

$$\tilde{\omega} = \frac{\bar{\omega}}{Ma} = t_\sigma / t_\omega. \quad (7.3)$$

If either the frequency parameter (2.11) or the Marangoni parameter (2.9) is small, equation (7.1) can be solved by perturbation in  $Ma^{-1}$  or  $\bar{\omega}^{-1}$  with parameters  $\hat{\lambda}$  and  $\tilde{\omega}$  fixed. The resulting expansions

$$\gamma_{lm,k} = \sum_{p=1}^{\infty} Ma^{-p} \gamma_{lm,k}^{(p)}(\tilde{\omega}, \hat{\lambda}) \quad (7.4)$$

and

$$\gamma_{lm,k} = \sum_{p=1}^{\infty} \bar{\omega}^{-p} \tilde{\gamma}_{lm,k}^{(p)}(\tilde{\omega}, \hat{\lambda}) \quad (7.5)$$

are related by

$$\tilde{\gamma}_{lm,k}^{(p)}(\tilde{\omega}, \hat{\lambda}) = \tilde{\omega}^p \gamma_{lm,k}^{(p)}(\tilde{\omega}, \hat{\lambda}). \quad (7.6)$$

The expansion coefficients  $\gamma_{lm,k}^{(p)}$  satisfy the perturbation equations

$$\gamma_{2m,k}^{(1)} = -i \frac{m}{2} \left( \frac{3}{10} \pi \right)^{1/2} \left[ ik\tilde{\omega} - \frac{6}{5} \right]^{-1} \delta_{|m|2} \delta_{|k|1}, \quad (7.7)$$

$$\begin{aligned} \gamma_{lm,k}^{(p+1)} = [ik\tilde{\omega} - W(l)]^{-1} & \left\{ \frac{1}{4} im\hat{\lambda} (\gamma_{lm,k-1}^{(p)} + \gamma_{lm,k+1}^{(p)}) + \frac{1}{2} A_{lm'l'm'} (\gamma_{l'm',k-1}^{(p)} + \gamma_{l'm',k+1}^{(p)}) \right. \\ & \left. + \Theta_{lm'l'm''} \sum_{j=0}^p \sum_{s=-\infty}^{+\infty} \gamma_{l''m'',k-s}^{(j)} \gamma_{l'm',s}^{(p-j)} \right\}, \quad (7.8) \end{aligned}$$

and

$$\gamma_{lm,k}^{(p)} = 0 \quad \text{for } l > 2p \quad \text{or} \quad |k| > p. \quad (7.9)$$

For  $\hat{\lambda}$  fixed, the expansion converges uniformly in  $Ma^{-1}$  for all  $\tilde{\omega}$ . Note however that corotational invariance is not preserved.

The expansions in  $Ma^{-1}$  of the real Fourier modes (5.3) and (5.4) for the surfactant contributions to the shear and normal stresses,

$$\eta'_{2n+1} = \sum_{r=n}^{\infty} Ma^{-2r} \eta_{2n+1}^{(2r)}, \quad (7.10)$$

$$\eta''_{2n+1} = \sum_{r=n}^{\infty} Ma^{-2r} \eta_{2n+1}^{\prime\prime(2r)}, \quad (7.11)$$

$$N'_{i,2n} = \sum_{r=\max(0,n-1)}^{\infty} Ma^{-(2r+1)} N_{i,2n}^{\prime(2r+1)}, \quad n \geq 0, \quad (7.12)$$

$$N''_{i,2n} = \sum_{r=n-1}^{\infty} Ma^{-(2r+1)} N''_{i,2n}^{(2r+1)}, \quad n > 0, \quad (7.13)$$

are obtained by inserting relations (7.2) and (7.4) into (3.5)–(3.7). Only even powers of  $Ma^{-1}$  contribute to  $\tau_{12}^r$  and odd powers of  $Ma^{-1}$  contribute to  $N_i$ , because the shear stress changes sign and the normal stresses are invariant under the transformation  $(x, y, z) \rightarrow (-x, y, -z)$  associated with the reversal of the imposed flow (2.3). The complementary expansions in  $\bar{\omega}^{-1}$  are obtained using relation (7.6).

### 7.1. Weakly nonlinear rheological response

At leading order in  $Ma^{-1}$  the response of the system is linear: normal stresses vanish, and only the fundamental  $k = 1$  Fourier mode contributes to the shear stress (5.3). The leading-order expansion coefficients for the shear stress are

$$\eta_1^{(0)} = \tau_{\max} \frac{1}{1 + t_0^2 \omega^2}, \quad (7.14)$$

$$\eta_1^{\prime(0)} = \tau_{\max} \frac{t_0 \omega}{1 + t_0^2 \omega^2}, \quad (7.15)$$

where  $\tau_{\max}$  and  $t_0$  are given by equations (2.21) and (6.16). At  $O(Ma^{-1})$ , the  $k = 0, 2$  modes appear in the Fourier expansion (5.4) of the normal stresses,

$$N_{1,0}^{\prime(1)} = \frac{5}{4} \frac{1}{1 + (t_0 \omega)^2}, \quad (7.16)$$

$$N_{1,2}^{\prime(1)} = \frac{5}{4} \left[ -\frac{1}{1 + (t_0 \omega)^2} + \frac{2}{1 + (2t_0 \omega)^2} \right], \quad (7.17)$$

$$N_{1,2}^{\prime\prime(1)} = \frac{5}{4} t_0 \omega \left[ -\frac{1}{1 + (t_0 \omega)^2} + \frac{4}{1 + (2t_0 \omega)^2} \right], \quad (7.18)$$

$$N_{2,0}^{(1)} = 0, \quad (7.19)$$

$$N_{2,2}^{\prime(1)} = \hat{\lambda}^{-1} \frac{15}{28} \left[ \frac{1}{1 + (t_0 \omega)^2} - \frac{1}{1 + (2t_0 \omega)^2} \right], \quad (7.20)$$

$$N_{2,2}^{\prime\prime(1)} = \hat{\lambda}^{-1} \frac{15}{28} t_0 \omega \left\{ \frac{1}{[1 + (t_0 \omega)^2]^2} + \frac{1}{2} \frac{1}{1 + (t_0 \omega)^2} - \frac{2}{1 + (2t_0 \omega)^2} \right\}. \quad (7.21)$$

Expressions for the shear and normal stresses at the next two perturbation levels are listed in Appendix C. Equations (7.14)–(7.21) are equivalent to the leading-order terms in the frequency expansion of the corotational Maxwell model, because up to  $O(Ma^{-1})$ , the coefficients  $\gamma_{2m,k}$  do not couple to  $\gamma_{l'm',k'}$  with  $l' \neq 2$ .

### 7.2. Comparison with numerical results

In figures 5 and 6, the leading-order results obtained from the small Marangoni/frequency parameter expansion (7.10)–(7.13) are shown for several Fourier modes of the shear and normal stresses. The results indicate that the expansion converges rapidly for  $\bar{\omega}^{-1} \leq O(1)$ ; for larger values of  $\bar{\omega}^{-1}$ , the expansion diverges because the Marangoni parameter used for this example is not small ( $Ma^{-1} = 1$ ).

## 8. Conclusions

We have shown that the interplay between the three dimensionless time-scale parameters gives rise to a rich rheological behaviour in diluted emulsions with surfactant-covered spherical drops. The parameters correspond to the Marangoni relaxation time, rotation time, and period of imposed flow oscillations normalized by the time scale for distortion of the surfactant distribution by the straining component of the flow. These parameters thus describe the relative strengths of the mechanisms that control the magnitude of surfactant redistribution; the dominant restoring mechanism is associated with the smallest parameter value. Multiple restoring mechanisms are evident in the response of the system when their time scales are distinct.

The focus in this paper is on diluted suspensions of surfactant-covered emulsion drops. However, the interplay between microstructural relaxation and externally imposed time scales also arises in other complex fluid systems. For example, dimpled shear-stress profiles, as shown in figure 3(a, b), have been observed in phase-separating polymer blends (Chopra, Vlassopoulos & Hatzikiriakos 2000), and block copolymer gels (Hamley *et al.* 1998) undergoing low-frequency oscillatory flow; transient shear stress oscillations, as seen in figure 1(c), have been observed in micellar solutions upon start-up of shear flow (Berret *et al.* 1995). This feature reflects shear thinning resulting from flow-induced alignment of the microstructure, as discussed in the text. The theory developed herein may thus help to interpret a number of non-equilibrium phenomena that result from the interaction of intrinsic and imposed time scales in complex fluids.

P. V. was supported by NSF grant CTS-9624615, and J. B. was supported by NASA grant NAG3-1935.

## Appendix A. Matrices $\mathcal{A}$ and $\Theta$

According to the results in I, the matrix elements of the matrices  $\mathcal{A}$  and  $\Theta$  in equation (3.2) are given by

$$\mathcal{A}_{lm'l'm'} = \mp i \left[ \frac{1}{3} \pi l(l+1) \right]^{1/2} \mathcal{S}(l, m | 2, \pm 2; l', m'), \quad (\text{A } 1)$$

$$\Theta_{lm'l''m''} = [l'(l'+1)]^{-1/2} \mathcal{S}(l, m | l'', m''; l' m') W(l'), \quad (\text{A } 2)$$

where the coupling coefficients  $\mathcal{S}$  are

$$\begin{aligned} \mathcal{S}(l, m | l', m'; l'' m'') &= \frac{(-1)^m}{2} \left[ \frac{(2l+1)(2l'+1)(2l''+1)}{4\pi} \right]^{1/2} \\ &\quad \times \begin{pmatrix} l' & l'' & l \\ m' & m'' & -m \end{pmatrix} \begin{pmatrix} l & l' & l'' \\ 0 & 0 & 0 \end{pmatrix}, \quad (\text{A } 3) \end{aligned}$$

and  $\begin{pmatrix} l & l' & l'' \\ m & m' & m'' \end{pmatrix}$  is the Wigner  $3j$ -symbol (Edmonds 1960). The  $3j$ -symbol vanishes,

$$\begin{pmatrix} l & l' & l'' \\ m & m' & m'' \end{pmatrix} = 0, \quad (\text{A } 4)$$

unless

$$m + m' + m'' = 0, \quad (\text{A } 5)$$

and the triangular condition

$$-l + l' + l'' \geq 0, \quad l - l' + l'' \geq 0, \quad l + l' - l'' \geq 0 \quad (\text{A } 6)$$

is satisfied. Also,

$$\begin{pmatrix} l & l' & l'' \\ 0 & 0 & 0 \end{pmatrix} = 0, \quad (\text{A } 7)$$

unless

$$l + l' + l'' = 2k, \quad k = 1, 2, \dots \quad (\text{A } 8)$$

### Appendix B. Higher-order terms in the corotational expansion for impulsively started flow

The  $O(\hat{\lambda}^{-3})$  terms in the expansion (6.8)–(6.10) for the stress evolution upon the inception of steady shear flow were derived by integrating the perturbation equations (6.5)–(6.6) with flow amplitude (4.1), and using relations (3.5)–(3.7). The partial-fraction expansion of the resulting expressions involves poles in the complex Marangoni-parameter plane,

$$\mathcal{P}_p(\tilde{M}a^{-1}) = \frac{1}{1 + p^2 \tilde{M}a^{-2}}, \quad (\text{B } 1)$$

and relaxation times

$$\left. \begin{aligned} t_0 &= p_1 \tilde{M}a^{-1}, & t_1 &= \frac{1}{2} p_1 \tilde{M}a^{-1}, & t_2 &= \frac{1}{3} p_1 \tilde{M}a^{-1}, \\ t_3 &= \frac{1}{2} p_2 \tilde{M}a^{-1}, & t_4 &= (p_1 + \frac{1}{2} p_2)^{-1} \tilde{M}a^{-1}, \end{aligned} \right\} \quad (\text{B } 2)$$

where

$$p_1 = \frac{5}{6}, \quad p_2 = \frac{9}{10}, \quad p_3 = \frac{45}{46}, \quad (\text{B } 3)$$

and  $p = p_i$  in equation (B 1).

The  $O(\hat{\lambda}^{-3})$  contribution to the shear stress has the form

$$\begin{aligned} \tau_{12}^{(3)}(t) &= \tau_{12}^{(3), \text{stat}} + \exp\left(-\frac{t}{t_0}\right) \{t[G_0^c \cos(t) + G_0^s \sin(t)] + F_0^c \cos(t) + F_0^s \sin(t)\} \\ &+ \exp\left(-\frac{t}{t_1}\right) [F_1 + F_1^c \cos(2t) + F_1^s \sin(2t)] + \exp\left(-\frac{t}{t_2}\right) F_2[-\cos(t) + t_0 \sin(t)] \\ &+ \exp\left(-\frac{t}{t_3}\right) [F_3 + F_3^c \cos(2t) + F_3^s \sin(2t)] + \exp\left(-\frac{t}{t_4}\right) [F_4^c \cos(t) + F_4^s \sin(t)], \end{aligned} \quad (\text{B } 4)$$

where

$$\tau_{12}^{(3), \text{stat}} = \frac{645}{28} \mathcal{P}_{5/6}^3 + \frac{11715}{112} \mathcal{P}_{5/6}^2 + \frac{9060195}{11648} \mathcal{P}_{5/6} - \frac{10546875}{11648} \mathcal{P}_{9/10} \quad (\text{B } 5)$$

is the stationary long-time value (which is equivalent to the results in I). The remaining

coefficients in equation (B 4) are

$$\begin{aligned}
 G_0^c &= t_0 \left( \frac{645}{28} \mathcal{P}_{5/6}^2 + \frac{602127}{9800} \mathcal{P}_{5/6} - \frac{19317771}{225400} \mathcal{P}_{45/46} \right), \\
 G_0^s &= \frac{645}{28} \mathcal{P}_{5/6}^2 + \frac{975279}{19600} \mathcal{P}_{5/6} - \frac{1427679}{19600} \mathcal{P}_{45/46}, \\
 F_0^c &= -\frac{174987}{1225} \mathcal{P}_{5/6}^2 - \frac{1205058087}{1592500} \mathcal{P}_{5/6} - \frac{10125}{1664} \mathcal{P}_{9/10} - \frac{715473}{4900} \mathcal{P}_{45/46}^2 \\
 &\quad + \frac{4122485793}{3920000} \mathcal{P}_{45/46}, \\
 F_0^s &= t_0 \left( \frac{203403}{1400} \mathcal{P}_{5/6}^2 + \frac{21384067767}{25480000} \mathcal{P}_{5/6} - \frac{10935}{1664} \mathcal{P}_{9/10} + \frac{1675971}{9800} \mathcal{P}_{45/46}^2 \right. \\
 &\quad \left. - \frac{103581379989}{90160000} \mathcal{P}_{45/46} \right), \\
 F_1 &= -\frac{255}{112} \mathcal{P}_{5/6}^2 - \frac{81273}{22400} \mathcal{P}_{5/6} + \frac{132273}{22400} \mathcal{P}_{45/46}, \\
 F_1^c &= -\frac{645}{28} \mathcal{P}_{5/6}^3 + \frac{96699}{2450} \mathcal{P}_{5/6}^2 - \frac{32222241}{1960000} \mathcal{P}_{5/6} + \frac{1863}{280000} \mathcal{P}_{45/46}, \\
 F_1^s &= t_0 \left( \frac{645}{28} \mathcal{P}_{5/6}^3 - \frac{273921}{9800} \mathcal{P}_{5/6}^2 + \frac{1348413}{280000} \mathcal{P}_{5/6} + \frac{2187}{280000} \mathcal{P}_{45/46} \right), \\
 F_2 &= \frac{207}{196} t_0^2 \mathcal{P}_{5/6}^2, \\
 F_3 &= -\frac{50301}{560000} \mathcal{P}_{5/6} + \frac{3267}{19600} \mathcal{P}_{45/46}^2 - \frac{301293}{3920000} \mathcal{P}_{45/46}, \\
 F_3^c &= \frac{2187}{8320} \mathcal{P}_{5/6} + \frac{10546875}{11648} \mathcal{P}_{9/10} + \frac{16335}{112} \mathcal{P}_{45/46}^2 - \frac{1177767}{1120} \mathcal{P}_{45/46}, \\
 F_3^s &= t_3 \left( \frac{405}{832} \mathcal{P}_{5/6} - \frac{10546875}{5824} \mathcal{P}_{9/10} - \frac{408375}{1288} \mathcal{P}_{45/46}^2 + \frac{1370115}{644} \mathcal{P}_{45/46} \right), \\
 F_4^c &= -\frac{19683}{113750} \mathcal{P}_{5/6} + \frac{10125}{1664} \mathcal{P}_{9/10} - \frac{3310551}{560000} \mathcal{P}_{45/46}, \\
 F_4^s &= t_4 \left( -\frac{523017}{520000} \mathcal{P}_{5/6} - \frac{31185}{1664} \mathcal{P}_{9/10} + \frac{1579743}{80000} \mathcal{P}_{45/46} \right).
 \end{aligned} \tag{B 6}$$

The  $O(\hat{\lambda}^{-3})$  term in the expansion (6.9) for the first normal stress difference has a similar structure and is available upon request from the JFM Editorial office, Cambridge.

### Appendix C. Higher-order terms in the small Marangoni/frequency parameter expansion

In this Appendix we give the  $O(Ma^{-2})$  terms in the expansion (7.10)–(7.11) for the Fourier modes of the stress tensor. The results were obtained by integrating the perturbation equations (7.7)–(7.8), and using relation (3.5). The partial-fraction expansions of the resulting expressions involves the poles in the complex frequency-

parameter plane,

$$\mathcal{P}_p(\tilde{\omega}) = \frac{1}{1 + p^2 \tilde{\omega}^2}, \quad (\text{C } 1)$$

where

$$p = \frac{5}{6}, \frac{5}{3}, \frac{9}{10}, \frac{5}{2}, \frac{10}{3}, \frac{9}{20}, \frac{27}{20}. \quad (\text{C } 2)$$

The  $O(Ma^{-2})$  terms in the expansions (7.10) and (7.11) are

$$\begin{aligned} \hat{\lambda}\eta_1^{(2)} = & -\frac{3225}{784}\mathcal{P}_{5/6}^3 - \frac{71525}{3136}\mathcal{P}_{5/6}^2 + \frac{25}{96}\left(\hat{\lambda}^2 - \frac{6328333}{10192}\right)\mathcal{P}_{5/6} \\ & - \frac{25}{24}\left(\hat{\lambda}^2 - \frac{1}{49}\right)\mathcal{P}_{5/3} + \frac{61509375}{326144}\mathcal{P}_{9/10}, \end{aligned} \quad (\text{C } 3)$$

$$\begin{aligned} \hat{\lambda}\eta_1^{(2)}/\tilde{\omega} = & -\frac{5375}{1568}\mathcal{P}_{5/6}^3 - \frac{389875}{18816}\mathcal{P}_{5/6}^2 + \frac{125}{288}\left(\hat{\lambda}^2 - \frac{6834791}{20384}\right)\mathcal{P}_{5/6} \\ & - \frac{125}{72}\left(\hat{\lambda}^2 - \frac{1}{49}\right)\mathcal{P}_{5/3} + \frac{110716875}{652288}\mathcal{P}_{9/10}, \end{aligned} \quad (\text{C } 4)$$

$$\begin{aligned} \hat{\lambda}\eta_3^{(2)} = & \frac{575}{784}\mathcal{P}_{5/6}^3 + \frac{15875}{3136}\mathcal{P}_{5/6}^2 - \frac{25}{192}\left(\hat{\lambda}^2 - \frac{1077}{4}\right)\mathcal{P}_{5/6} + \frac{25}{24}\left(\hat{\lambda}^2 - \frac{9}{49}\right)\mathcal{P}_{5/3} \\ & - \frac{75}{64}\left(\hat{\lambda}^2 - \frac{267}{1568}\right)\mathcal{P}_{5/2} - \frac{4100625}{100352}\mathcal{P}_{9/10}, \end{aligned} \quad (\text{C } 5)$$

$$\begin{aligned} \hat{\lambda}\eta_3^{(2)}/\tilde{\omega} = & \frac{2875}{4704}\mathcal{P}_{5/6}^3 + \frac{28375}{6272}\mathcal{P}_{5/6}^2 - \frac{125}{1152}\left(\hat{\lambda}^2 - \frac{56997}{196}\right)\mathcal{P}_{5/6} \\ & + \frac{125}{72}\left(\hat{\lambda}^2 - \frac{9}{49}\right)\mathcal{P}_{5/3} - \frac{375}{128}\left(\hat{\lambda}^2 - \frac{267}{1568}\right)\mathcal{P}_{5/2} - \frac{7381125}{200704}\mathcal{P}_{9/10}, \end{aligned} \quad (\text{C } 6)$$

The  $O(Ma^{-3})$  terms in the expansions (7.12)–(7.13) have been derived and have similar structure. These are available upon request from the JFM Editorial office, Cambridge.

#### REFERENCES

- BERRET, J. F., ROUX, D. C., PORTE, G. & LINDNER, P. 1995 Tumbling behaviour of nematic worm-like micelles under shear flow. *Europhys. Lett.* **32**, 137–142.
- BIRD, R., ARMSTRONG, R. C. & HASSAGER, O. 1977 *Dynamics of Polymeric Liquids*, vol. 1. Wiley.
- BŁAWZDZIEWICZ, J., CRISTINI, V. & LOEWENBERG, M. 1999 Stokes flow in the presence of a planar interface covered with incompressible surfactant. *Phys. Fluids* **11**, 251–258.
- BŁAWZDZIEWICZ, J., VLAHOVSKA, P. & LOEWENBERG, M. 2000 Rheology of a dilute emulsion of surfactant-covered spherical drops. *Physica A* **276**, 50–80 (referred to herein as I).
- BŁAWZDZIEWICZ, J., WAJNRYB, E. & LOEWENBERG, M. 1999 Hydrodynamic interactions and collision efficiencies of spherical drops covered with an incompressible surfactant film. *J. Fluid Mech.* **395**, 29–59.
- CHOPRA, D., VLASSOPOULOS, D. & HATZIKIRIAKOS, S. 2000 Nonlinear rheological response of phase separating polymer blends: Poly(styrene-co-maleic anhydride)/poly(methyl methacrylate). *J. Rheol.* **44**, 27–45.
- DANOV, K. D. 2001 On the viscosity of dilute emulsions. *J. Colloid Interface Sci.* **235**, 144.
- EDMONDS, A. R. 1960 *Angular Momentum in Quantum Mechanics*. Princeton University Press.
- FLUMERFELT, R. W. 1980 Effects of dynamic interfacial properties on drop deformation and orientation in shear and extensional flow fields. *J. Colloid Interface Sci.* **76**, 330–349.

- HAMLEY, I. W., POPLE, J. A., BOOTH, C., DERICI, L., IMPÉROUR-CLERC, M. & DAVIDSON, P. 1998 Shear-induced orientation of the body-centered-cubic phase in a diblock copolymer gel. *Phys. Rev. E* **58**, 7620–7628.
- HOROZOV, T. & ARNAUDOV, L. 2000 Adsorption kinetics of some polyethylene glycol octylphenyl ethers studied by the fast formed drop technique. *J. Colloid Interface Sci.* **222**, 146–155.
- LEVICH, V. G. 1962 *Physicochemical Hydrodynamics*. Prentice–Hall.
- LI, X. & POZRIKIDIS, C. 1997 The effect of surfactants on drop deformation and on the rheology of dilute emulsions in Stokes flow. *J. Fluid Mech.* **341**, 165–194.
- MALDARELLI, C. & HUANG, W. 1996 The effect of surfactants on the motion of bubbles and drops. In *Flow of Particles in Suspensions* (ed. U. Schafflinger), pp. 125–160. Springer.
- OLDROYD, J. G. 1955 The effect of interfacial stabilizing films on the elastic and viscous properties of emulsions. *Proc. R. Soc. Lond. A* **232**, 567–577.
- PALIERNE, J. F. 1990 Linear rheology of viscoelastic emulsions with interfacial tension. *Rheol. Acta* **29**, 204–214, and correction *Rheol. Acta* **30** (1991), 497.
- PAWAR, Y. & STEBE, K. J. 1996 Marangoni effects on drop deformation in an extensional flow: The role of surfactant physical chemistry. I. Insoluble surfactants. *Phys. Fluids* **8**, 1738–1751.
- RALLISON, J. M. 1980 Note on the time-dependent deformation of a viscous drop which is almost spherical. *J. Fluid Mech.* **98**, 625–633.
- RAO, B. N., TANG, L. & ALTAN, M. C. 1994 Rheological properties of non-Brownian spheroidal particle suspensions. *J. Rheol.* **38**, 1335–1351.
- STONE, H. A. & LEAL, L. G. 1990 The effects of surfactants on drop deformation and breakup. *J. Fluid Mech.* **220**, 161–186.
- SZERI, A. J. & LIN, D. J. 1996 A deformation tensor model of Brownian suspensions of orientable particles—the nonlinear dynamics closure models. *J. Non-Newtonian Fluid Mech.* **64**, 43–69.
- TAYLOR, G. I. 1932 The viscosity of a fluid containing small drops of another fluid. *Proc. R. Soc. Lond. A* **138**, 41.
- YON, S. & POZRIKIDIS, C. 1998 A finite-volume/boundary-element method for flow past interfaces in the presence of surfactants, with application to shear flow past a viscous drop. *Computers Fluids* **27**, 879–902.